Article

High-Power, High-Purity HG_{0n} Hermite–Gaussian Laser Beam Generation in Cascaded Large Aspect Ratio Slabs

Tianli Yang [1,2,3], Jing Yang [1,2,*], Wangzhe Zhou [1,2,3], Xuepeng Li [1,2], Yinan Zhou [1,2,3], Zongzhe Zhang [1,2] and Xiaojun Wang [1,2,*]

[1] Key Laboratory of Solid-State Laser, Technical Institute of Physics and Chemistry, Chinese Academy of Sciences, Beijing 100190, China; yangtianli18@mails.ucas.ac.cn (T.Y.); zhouwangzhe20@mails.ucas.ac.cn (W.Z.); lixuepeng@mail.ipc.ac.cn (X.L.); zoyina35@163.com (Y.Z.); zhangzongzhe@mail.ipc.ac.cn (Z.Z.)

[2] Key Laboratory of Functional Crystal and Laser Technology, Technical Institute of Physics and Chemistry, Chinese Academy of Sciences, Beijing 100190, China

[3] University of Chinese Academy of Sciences, Beijing 100190, China

* Correspondence: yangjing@mail.ipc.ac.cn (J.Y.); wangxj@mail.ipc.ac.cn (X.W.); Tel.: +86-10-82543547 (J.Y. & X.W.)

Featured Application: The one-dimensional, high-order Hermite–Gaussian (HG_{0n}) laser beams can be easily converted into vortex Laguerre–Gaussian (LG_{pl}) beams carrying orbital angular momentum (OAM), and with the scaling of output power and the narrowing of pulse width, the applications of HG_{0n} laser beams have been expanded from original cutting-edge scientific scenarios to optical measurement, material processing, aerospace communication, and many other fields.

Abstract: High-power, high-purity, nanosecond (ns) one-dimensional HG_{0n} laser beams are proposed and demonstrated by using Nd:YAG cascaded slabs with a large aspect ratio. The HG_{0n} laser beams are generated by adjusting the pump distribution, the intracavity apertures, and the tilt angle of the output coupler (OC). By controlling the gain and loss of HG_{0n} modes of different orders, the high-purity, one-dimensional, high-order HG_{0n} laser beams with orders 1 to 9 (HG_{01} to HG_{09}) are produced, and their beam quality factors M^2 align well with the theoretical predictions. Meanwhile, the large aspect ratio slab provides an ideal amplifier for the strip-shaped HG_{0n} laser beams, and further power scaling is achieved by seeding the generated HG_{0n} laser beams into an amplifier with an identical slab module. For the HG_{09} mode, the average power is amplified from 289 mW to 4.73 W with 294 ns pulse width, corresponding to a peak power of 32 kW. Moreover, above 5 W average power is achieved for all HG_{01} to HG_{08} modes. Hopefully, this scheme provides a solution for high-power and high-purity HG_{0n} laser beam generation based on the slab-shaped configuration.

Keywords: Hermite–Gaussian beam; slab laser; master oscillator power amplifier (MOPA); Q-switched

1. Introduction

Hermite–Gaussian (HG_{mn}) laser beams, with specific intensity and phase distribution, have potential applications in many cutting-edge scientific scenarios [1–5]. The typical methods for generating HG_{mn} laser beams are off-axis diode-end-pumping gain modules [6–8] or inserting specific optical components such as a spiral phase plate [9] and spatial light modulator [10] in the laser cavity. Generally, the output power of most HG_{mn} laser beams is only one watt level or less. For example, a 265 mW average power and 1.7 kW peak power HG_{mn} laser beam was obtained using a passively Q-switched Nd:YVO$_4$ microchip laser based on off-axis pumping [11]. In another work, an average power of less than 1.3 W with nanosecond (ns) pulse width and ~4 kW peak power has been achieved in a decentered Gaussian beam pumped Q-switched Nd:YAG microchip laser for different high-order transverse modes [12].

A one-dimensional high-order HG_{0n} laser beam is a typical HG_{mn} laser beam, where $m = 0$. This means no dark bars are crossing the pattern in the x-direction, while the number

of dark bars in the y-direction is n, so the HG_{0n} laser beams display as strip shape. Due to the fact that HG_{0n} laser beams can be easily converted into vortex Laguerre–Gaussian (LG_{pl}) beams carrying orbital angular momentum (OAM) by adopting the Astigmatic Mode Converter (AMC), the applications of HG_{mn} laser beams have been further expanded [13–15], and the HG_{0n} laser beams with both high average power and high peak power are expected to be obtained.

As is well known, for the most commonly used off-axis pumping method, the radius of the pump beam with about a one-hundred-micrometer level is much smaller than the spot of the one-dimensional high-order HG_{0n} mode beams, then the intensity of the HG_{0n} mode beams inside and outside the pumping region is different. Consequently, the purity of the HG_{0n} laser beams should be significantly reduced. On the other hand, in order to obtain HG_{0n} laser beams with higher power, higher pump power is required, which will lead to significant thermal lens effects and thus affect the mode of the laser. Therefore, the development of a new method for obtaining high-average-power and high-peak-power, high-purity HG_{0n} modes has become a hot research field.

Slabs with large aspect ratios have been widely used in laser systems because of their large gain volume, great pump uniformity, and favorable thermal management [16–18]. Since the zig-zag optical path in the slab averages the thermal gradient, there is almost no first-order thermal lens effect, making it a promising method for extracting higher power while simultaneously maintaining good beam quality. In this letter, an alternative method for generating a high-purity, one-dimensional HG_{0n} laser beam has been proposed and demonstrated. Different from traditional approaches, a Nd:YAG slab with a large aspect ratio of 7.5 is selected as the gain medium. By adjusting the pump intensity, the size of the aperture pair in thickness and width directions of the slab, and the tilt angle of the output coupler (OC), the intracavity mode is controlled, and high-purity, ns one-dimensional HG_{0n} laser beams with orders 1 to 9 (HG_{01} to HG_{09}) are obtained from the slab oscillator in Q-switched operation. The beam quality factors M^2 are in reasonable agreement with the theoretical values. Because the large aspect ratio slab provides an ideal amplifier for the strip-shaped HG_{0n} laser beam, further power scaling is realized. The seed beam from the oscillator is directly injected into the other identical slab as the amplifier. For the highest order HG_{09} mode beam, the average power is amplified from 289 mW to 4.73 W with a pulse width of 294 ns, corresponding to a peak power of 32 kW.

2. Theoretical Analysis

According to the mode theory of the optical resonator, the self-reproducing field pattern of a square aperture flat–concave resonator can be expressed in rectangular coordinates as [19]

$$u_{mn}(x,y,z) = \frac{C_{mn}}{w(z)} H_m\left(\frac{\sqrt{2}}{w(z)}x\right) H_n\left(\frac{\sqrt{2}}{w(z)}y\right) \exp\left(-\frac{x^2+y^2}{w(z)^2}\right)$$
$$\times \exp\left(-ik\frac{x^2+y^2}{2R(z)}\right) \exp[-i(m+n+1)\psi(z)], \tag{1}$$

where $w(z) = w_0\sqrt{1+z^2/z_R^2}$ is the beam radius on the axial position z; $R(z) = \left(z_R^2+z^2\right)/z$ is the radius of curvature of the wavefront that intersects the axis at z; C_{mn} is the normalization constant; w_0 is the radius of the fundamental mode Gaussian beam at $z = 0$, which can be calculated by the propagation matrix; $z_R = \pi w_0^2/\lambda$ is the Rayleigh range of the mode; and H_m and H_n are the mth- and nth-order Hermite polynomial, respectively. In the transverse field distribution, the number of nodes with zero intensity in the x- and y-directions are m and n, respectively, so that for the one-dimensional HG_{mn} beams mentioned in this letter, $m = 0$. The relationship between the radius of HG_{0n} mode and HG_{00} mode can be obtained from Equation (1) [20]:

$$w_{0n} = \sqrt{2n+1}\,w_{00}. \tag{2}$$

Combined with the ABCD propagation matrix, the beam radius of HG_{0n} mode at any position in the resonator can be calculated. Considering the ratio of the diameter of

the one-dimensional HG_{0n} beam in the x- and y-directions, the slab is selected as the gain medium due to the inherent advantage of its large aspect ratio.

To generate high-purity, one-dimensional HG_{0n} laser beams, the fundamental mode in the slab's thickness direction, i.e., the x-direction, needs to be determined first. A small aperture in the thickness direction of the slab provides an advantage for the fundamental mode output. On the other hand, an aperture that matches the diameter of the fundamental mode in the thickness direction of the slab can be inserted into the resonator to limit the transverse mode field in this direction; thus, only one-dimensional HG_{0n} laser beams exist in the cavity.

Then, the high-order mode in the slab's width (y-) direction must be ensured. Because the diameter of high-order modes is larger than that of the low-order mode, high-order modes can be suppressed using an intracavity aperture with proper width [20]. The width of the aperture used for mode-limiting is adjusted according to the theoretical mode diameter of its position to ensure the highest order of the HG_{0n} mode that can exist in the cavity is N. Due to the limitation of the aperture, only the HG_{00} to HG_{0N} modes exist in the cavity. The width ratio of the two apertures in the width and thickness direction is just suitable due to the large aspect ratio of the slab.

Furthermore, to extract the high-purity HG_{0N} mode from the HG_{00} to HG_{0N} modes, it is necessary to perform differential regulation on each order mode's gain G_{0n} and loss L_{0n}. It can be seen from Equation (2) that the higher-order mode has a larger mode volume and a greater overlap with the gain region so that for slab configuration, the higher-order mode can occupy more population inversion; that is, the gain G_{0n} is larger. On the other hand, when the Fresnel number of the resonator is determined, the diffraction loss of the higher-order mode is higher than that of the lower-order mode [21], so the threshold of the higher-order mode is generally higher than that of the low-order mode. But this can be changed by introducing OC tilt angles into the resonator. Previous studies have shown that for a given resonator, the misalignment of two cavity mirrors has less effect on higher-order modes [22]. The introduction of the tilt leads to an increase in the total loss L_{0n} of each mode in the cavity, but the increase in the loss of the higher-order mode is less than that of the lower-order mode. For a given aperture, there is a suitable tilt angle that prevents the lower-order modes from oscillating, and the highest-order mode HG_{0N} wins in the mode competition. However, when the pump power is high, each order mode in the resonator can obtain sufficient gain, G_{0n}, which causes the simultaneous resonation of each mode in the cavity, producing a multimode laser output. Therefore, in order to achieve specific high-order mode output, the pump power needs to be controlled at a reasonable level. Thus, their output power is limited for a single oscillator.

The master oscillator power amplifier (MOPA) effectively scales the output power of high-purity HG_{0n} laser beams. The slab with a large aspect ratio used in the amplifier provides an ideal condition for power scaling of strip-shaped HG_{0n} laser beams without additional beam shaping. Another advantage of using a slab as an amplification gain medium is the simplicity of thermal management. Since the zig-zag optical path in the slab averages the thermal gradient, there is almost no first-order thermal lens effect, making it a promising method for scaling laser output to higher power while simultaneously maintaining good beam quality.

3. Generation of High-Purity, Nanosecond HG_{0n} Laser Beams

The experimental setup of the oscillator for generating high-purity, nanosecond HG_{0n} laser beams is shown in Figure 1. The laser oscillator includes a laser module, a pair of apertures A_x and A_y, a rear cavity mirror M1, an OC M2, and an acousto-optic (AO) Q-switch. The laser module contains a 0.6 at. % doped trapezoidal Nd:YAG slab crystal with dimensions of 139 mm × 30 mm × 4 mm (length × width × thick), having a large aspect ratio of 7.5. The cut angle of the two end facets of the slab is 56°, and both are coated with anti-reflective (AR) film at 1064 nm. The top surface of the slab is coated with an AR film for 808 nm, and the bottom surface of the slab is highly reflective (HR) at 808 nm for

double-pass pumping. The top surface of the slab is edge-sealed with an O-ring, while the bottom surface is soldered on the oxygen-free copper heat sink with microchannels in order to maintain the temperature of the laser module at 20 °C (±0.2 °C) through a water cooler. The slab is face-pumped by six 808 nm quasi-continue-wave (QCW) microchannel-cooled laser diode arrays (LDA), with each array containing six bars. The temperature of cooling water for the LDA is tuned to 20 °C (±0.2 °C) to match the absorption spectrum of the crystal medium [23]. A pump beam with a 300 μs pump pulse duration and 500 Hz pulse repetition rate (PRR) is normally incident on the top face of the slab via a quartz duct. The size of the pump region is 66 mm × 20 mm, so the effective aspect ratio in the pump region is 20 mm/4 mm = 5. The laser beam propagates along a zig-zag optical path in the slab, and the internal reflection angle between the optical path and the normal of the bottom face of the slab is 56.0°. The rear cavity mirror M1 is a concave mirror with curvature radius R_1 of 1600 mm coated with HR film at 1064 nm. The output coupler M2 with a transmittance (T) of 10% is placed on a mount with an adjustable tilt angle, while the tilt angle θ in the y-o-z plane is the key to obtaining HG_{0n} laser beams. The AO Q-switch (SGQ27-1064-5QD, CETC) with a 5 mm × 5 mm active aperture is located in the front of the slab crystal. The arm lengths from the end facets of the slab to M_1 and A_y are L_1 = 110 mm and L_2 = 575 mm, respectively. Two apertures, A_x and A_y, with adjustable sizes in the thickness and width directions of the slab, are placed at L_x = 20 mm and L_y = 40 mm from M2, respectively. The total optical length of the resonator is 800 mm.
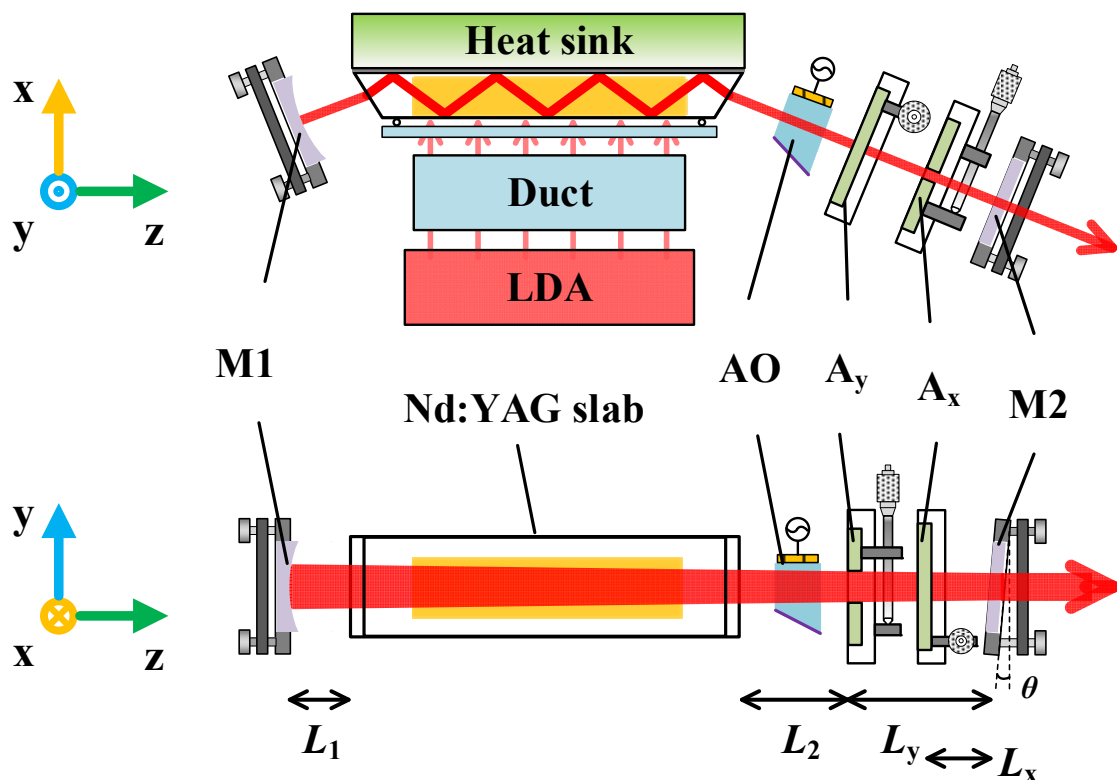

Figure 1. Schematic of the slab laser oscillator from top and side views. M1: rear cavity mirror; M2: output coupler; LDA: laser diode array; AO: acousto-optic Q-switch; A_x: aperture in the x-direction; A_y: aperture in the y-direction.

The sizes of apertures A_x and A_y in the thickness and width direction of the slab denote D_x and D_y, respectively. As mentioned above, D_x and D_y should be selected based on the resonator shown in Figure 1. Since the zig-zag optical path averages the thermal

gradient, the first-order thermal lens effect is almost ignored. The diameter of the beam at the position of A_y can be calculated by the ABCD propagation matrix, which is given by

$$
T = \begin{pmatrix} 1 & L_S + L_1 + L_2 - L_Q + \frac{L_Q}{n_q} \\ 0 & 1 \end{pmatrix} \begin{pmatrix} 1 & 0 \\ -\frac{2}{R_1} & 1 \end{pmatrix} \begin{pmatrix} 1 & L_S + L_1 \\ 0 & 1 \end{pmatrix}
$$
$$
\times \begin{pmatrix} 1 & L_2 - L_Q + \frac{L_Q}{n_q} + L_y \\ 0 & 1 \end{pmatrix} \begin{pmatrix} 1 & 0 \\ -\frac{2}{R_2} & 1 \end{pmatrix} \begin{pmatrix} 1 & L_y \\ 0 & 1 \end{pmatrix} = \begin{pmatrix} A & B \\ C & D \end{pmatrix} \tag{3}
$$

where $L_S = \frac{L}{n\cos(\alpha)}$ is the optical path length in the slab; L is the length of the Nd:YAG slab; n is the refractive index of Nd:YAG, which is 1.82; α is the angle between the laser path and the bottom surface of the slab; L_Q is the length of the AO Q-switch, which is 50 mm; n_q is the refractive index of the AO Q-switch, which is 1.45; and R_2 is the curvature radius of OC, which is taken as positive infinity in calculation. With the laser oscillator presented in Figure 1, the beam diameter, under the assumption of the fundamental mode, can be expressed by

$$
d_0 = 2\left(\frac{\lambda}{\pi}\right)^{\frac{1}{2}} |B|^{1/2} \left[1 - \left(\frac{D+A}{2}\right)^2\right]^{-1/4} \tag{4}
$$

where λ is the wavelength of the oscillating laser. Based on the beam diameter ratio between the HG_{0n} mode and the fundamental mode described in Equation (2), for a calculated 1.04 mm diameter fundamental mode at the position of A_y, the corresponding beam diameters of the HG_{01} to HG_{09} modes are about 1.80 mm, 2.33 mm, 2.76 mm, 3.13 mm, 3.45 mm, 3.76 mm, 4.04 mm, 4.30 mm, and 4.54 mm, respectively. Therefore, considering the 5 mm active aperture of the AO Q-switch, for the width direction of the slab, the width D_y of aperture A_y is adjusted to 2.0 mm, 2.4 mm, 3.0 mm, 3.4 mm, 3.8 mm, 4.0 mm, 4.3 mm, 4.5 mm, and 4.8 mm, respectively. A similar calculation is used to select the diameter D_x of the aperture A_x; in order to obtain the fundamental mode in the thickness direction of the slab, D_x is selected to be 1.3 mm.

A CMOS sensor (Beamage-4M, Gentec Inc., St-Jean-Baptiste, QC, CA) is used to record the intensity distribution of the output laser beams. The laser beams are focused by a lens with a 300 mm focal length. The tilt angle θ of OC M2 in the y-o-z plane is adjusted carefully, and then the beam intensity profile changes can be observed. When the HG_{0n} mode spatial profile with the strongest contrast is displayed on the CMOS at a given tilt angle θ, as shown in Table 1, the corresponding intensity distribution is recorded.

Table 1. Output power of HG_{01} to HG_{09} mode laser and corresponding OC tilt angle.

Mode	HG_{01}	HG_{02}	HG_{03}	HG_{04}	HG_{05}	HG_{06}	HG_{07}	HG_{08}	HG_{09}
P/mW	349.8	407.0	318.7	379.5	332.2	338.8	321.2	336.6	289.3
θ/mrad	0.636	0.022	0.678	0.107	0.512	0.520	0.121	0.095	0.750

A beam quality analyzer (Beamage-M2, Gentec Inc., St-Jean-Baptiste, QC, CA) measures the beam quality factors M^2 of the output laser beams at different apertures A_y and M2 tilt angles. Figure 2 shows the typical beam quality factors of the highest order HG_{09} mode in the x- and y-directions, which are $M_x^2 = 1.15$ (blue) and $M_y^2 = 19.96$ (red), respectively. The inset of Figure 2 displays the corresponding three-dimensional (3D) beam spatial intensity distribution at the far field, indicating nine intensity peaks.

Figure 3 shows the measured beam quality factors M_x^2 (blue triangle) and M_y^2 (red circle) of the HG_{01} to HG_{09} modes in the x- and y-directions, respectively. In Figure 3, it can be seen that the beam quality factors (M_x^2, M_y^2) of the HG_{01} to HG_{09} modes are (1.19, 3.44), (1.20, 5.58), (1.14, 7.09), (1.15, 9.98), (1.17, 11.20), (1.26, 13.39), (1.22, 15.79), (1.25, 17.10), and (1.15, 19.96), respectively. Considering the theoretical beam quality factor $M_x^2 = 1$ for the ideal fundamental mode in the x-direction and the beam quality factor $M_y^2 = 2n + 1$ for the

ideal HG_{0n} mode in the y-direction [24], the measured data are in reasonable agreement with the theoretical values. The corresponding two-dimensional (2D) intensity distribution is also shown in the insets of Figure 3, which exhibits high-purity HG_{0n} modes for orders 1 to 9. These results verify the feasibility of obtaining high-purity HG_{0n} laser beams by using a large aspect ratio Nd:YAG slab.
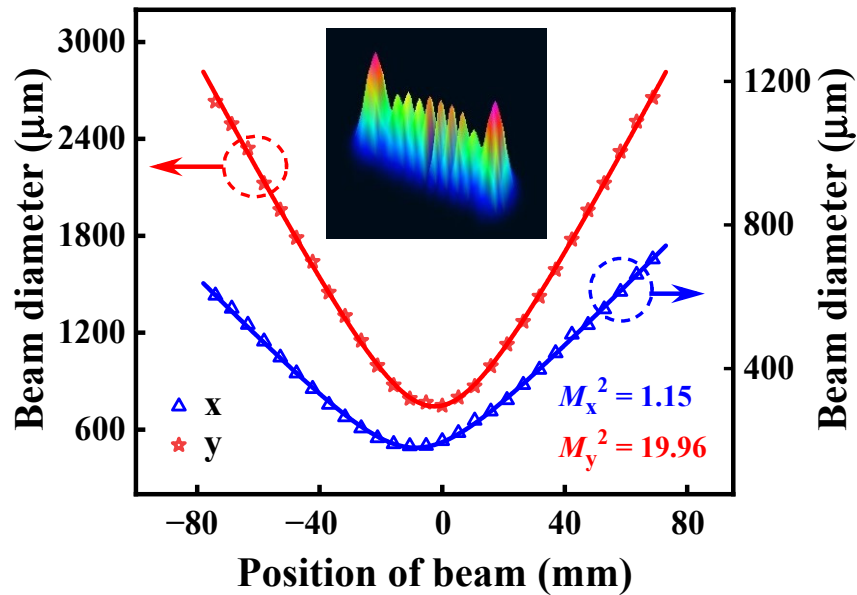

Figure 2. Measurement of beam quality factors M_x^2 (blue) and M_y^2 (red) of HG_{09} beam mode for the slab oscillator. Inset: far-field 3D beam spatial intensity distribution.
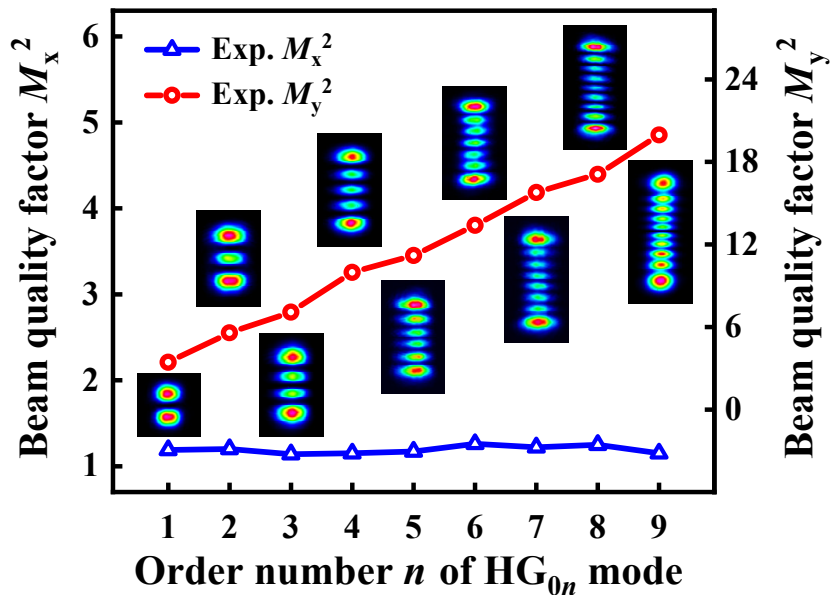

Figure 3. Beam quality factors M_x^2 and M_y^2 of the HG_{01} to HG_{09} modes. Inset: typical beam intensity distribution for the HG_{01} to HG_{09} modes.

The output power of the HG_{01} to HG_{09} modes is measured with a power meter (30A-BB-18, Ophir Inc., Jerusalem, Israel), and the results are shown in Table 1. It can be seen that the power is approximately 330 mW and fluctuates with the order, but for the highest order HG_{09} mode laser, the average power is about 289 mW. This is partly due to the larger tilt angle of the OC M2 in the y-o-z plane.

4. Power Scaling in MOPA System Using Cascaded Slab Module

The feasibility of power scaling is the inherited advantage of selecting a large aspect ratio slab module. A cascaded slab gain module is used for laser amplification. This amplification module is the same as the laser module mentioned earlier in the article, which includes a 0.6 at. % Nd^{3+} doped 139 mm × 45 mm × 4 mm (length × width × thick) trapezoidal Nd:YAG slab, a 6 × 6 LDA with 808 nm pump wavelength, 300 μs pump pulse duration and 500 Hz PRR, and a quartz duct. The temperature of the amplification module is also maintained at 20 °C (±0.2 °C). The experimental configuration scheme of the amplifier is shown in Figure 4a, and the picture illustrating the real system is also shown in Figure 4b. The seed pulse output from the oscillator is injected into the slab amplification module. To achieve higher energy extraction, a double-pass amplification geometry is adopted. The internal reflection angles between the two optical paths and the normal of the bottom face of the plate are 56.0° and 68.9°, respectively. The change in the optical path is due to the use of flat mirrors M3 and M4 coated with 35°~45° HR film at 1064 nm. After passing through the amplifier, the beam is divided into two parts by a beam splitter. The main part enters the power meter for the power measurement, and the leaking part is incident on CMOS to record the beam intensity distribution.
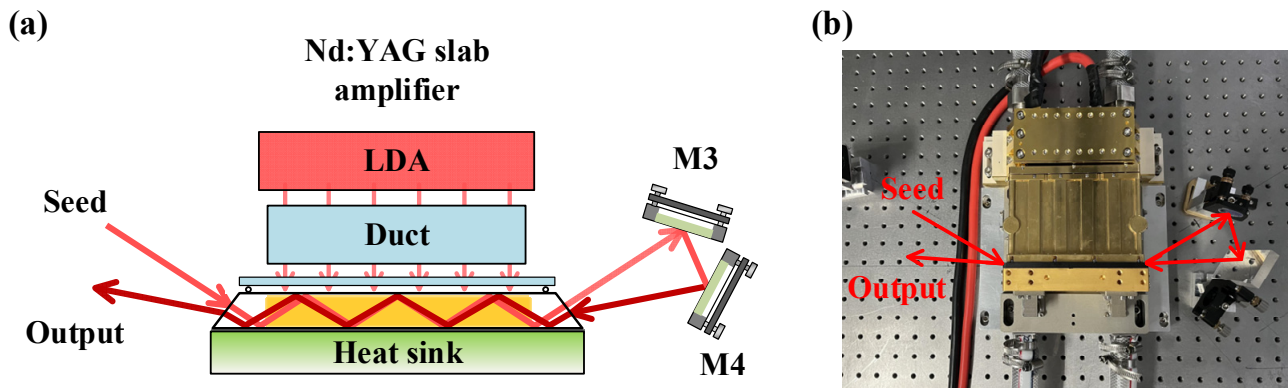

Figure 4. The double-pass slab amplifier. (**a**) The experimental configuration scheme of the amplifier. (**b**) The picture of the real system.

Figure 5 shows the amplified two-dimensional (2D) intensity distribution of HG_{01} to HG_{09} beam modes. Meanwhile, the normalized intensity curves (red) in the y-direction are shown in Figure 5, and the corresponding theoretical normalized intensity curves (blue) are also shown in Figure 5. In general, the experimental results are in reasonable agreement with the numerical simulation. Compared to the theoretical model, the slight intensity deviation of the beam in the experiment may be caused by the residual lower-order HG_{0n} modes.

The purity of the mode is described by using the Pearson correlation coefficient ρ:

$$\rho = \frac{\sum_{i=1}^{N} \left(I_i - \overline{I} \right) \left(I_i^* - \overline{I^*} \right)}{\sqrt{\sum_{i=1}^{N} \left(I_i - \overline{I} \right)^2} \sqrt{\sum_{i=1}^{N} \left(I_i^* - \overline{I^*} \right)^2}} \tag{5}$$

where I_i is the measured normalized intensity of each pixel, $\overline{I}$ is the average value of normalized intensities of all pixels, I_i^* is the normalized intensity obtained by the theoretical calculation, and $\overline{I^*}$ is the corresponding average value. The correlation coefficient of the highest order HG_{09} mode is calculated as $\rho_{09} = 0.944$, while the correlation coefficient of other modes $\rho_{0n} > 0.93$. It can be observed that the measured laser beams all have longer tails in the edge region of the x-direction. The diffraction effect of the intracavity aperture and the beam diffusion caused by the off-axis aberration of the cavity mirror are the reasons for the insufficient sharpness of the edge reduction.
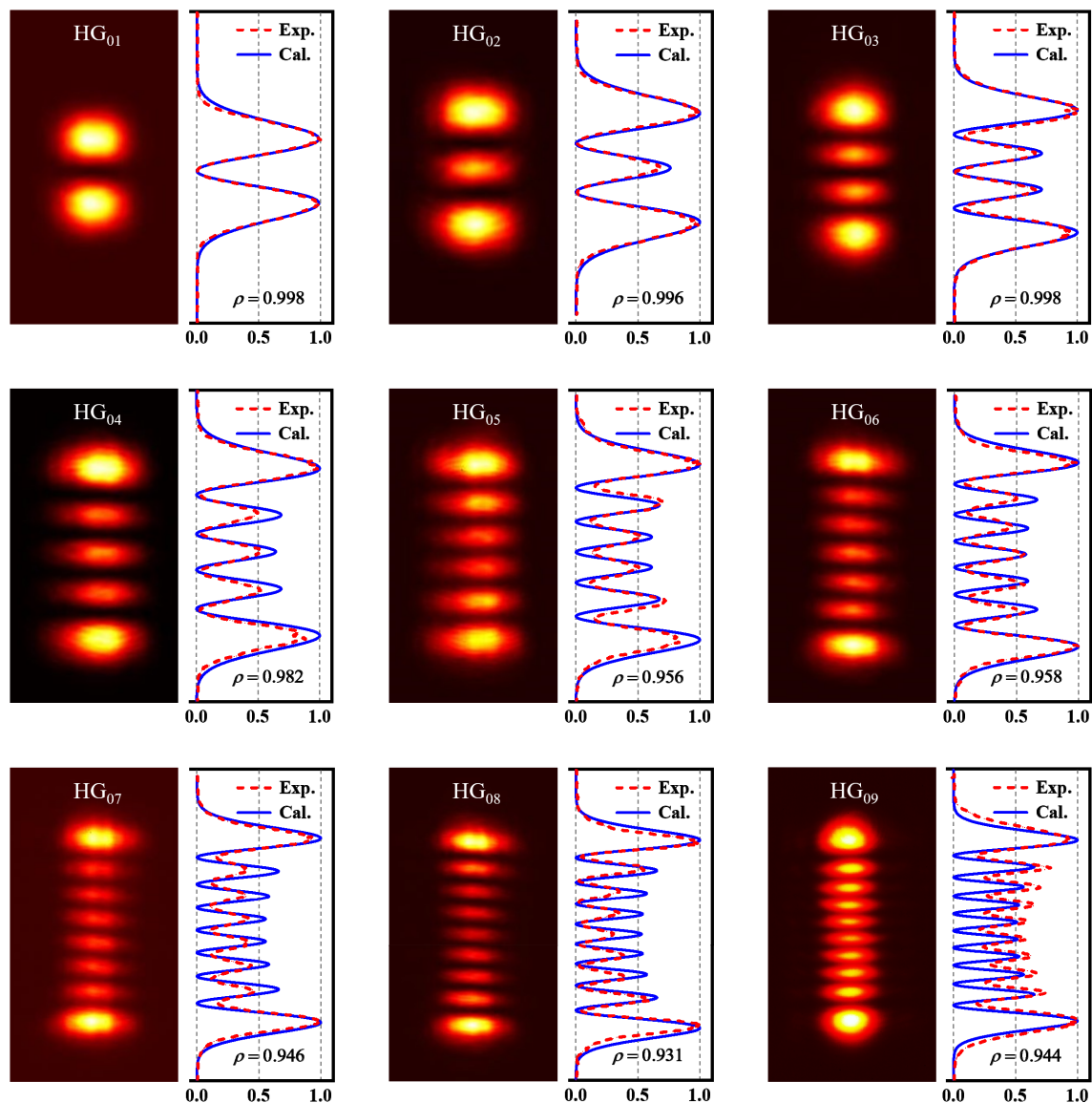
Figure 5. The 2D spatial beam profile and the corresponding normalized beam intensity carves of HG_{01} to HG_{09} mode after pulse amplification.

Figure 6a shows the amplified output power of typical mode HG_{09} (blue) versus the LD pump power. From Figure 6a, it can be seen the output power shows a monotonic increase with the incident pump power, amplifying from 289 mW to 4.73 W. The increase of output power is faster with the increase of the incident pump power and does not show any saturation effect up to around 850 W pump power. The amplified output powers of the HG_{01} to HG_{09} modes are also shown in Figure 6b, and it can be seen from Figure 6b that each output power from the HG_{01} to HG_{08} modes is higher than 5 W.

The pulse temporal characteristic of the amplified highest order HG_{09} mode is monitored by a photodiode detector (DET10N/M, Thorlabs Inc., Newton, NJ, USA) connected to a 200 MHz bandwidth digital oscilloscope (SDS1204X-E, SIGLENT Inc., Shenzhen, Guangdong, China), as shown in Figure 7 (red line). It was found that the pulse interval of the output pulse was 2 ms, indicating that the laser operated at a PRR of 500 Hz. The pulse-to-pulse amplitude fluctuation is less than 1.2% (Standard Deviation). The upper right inset of Figure 7 expresses an expanded single pulse profile (blue line), showing a pulse width of 295 ns, so the peak power corresponds to 32 kW.
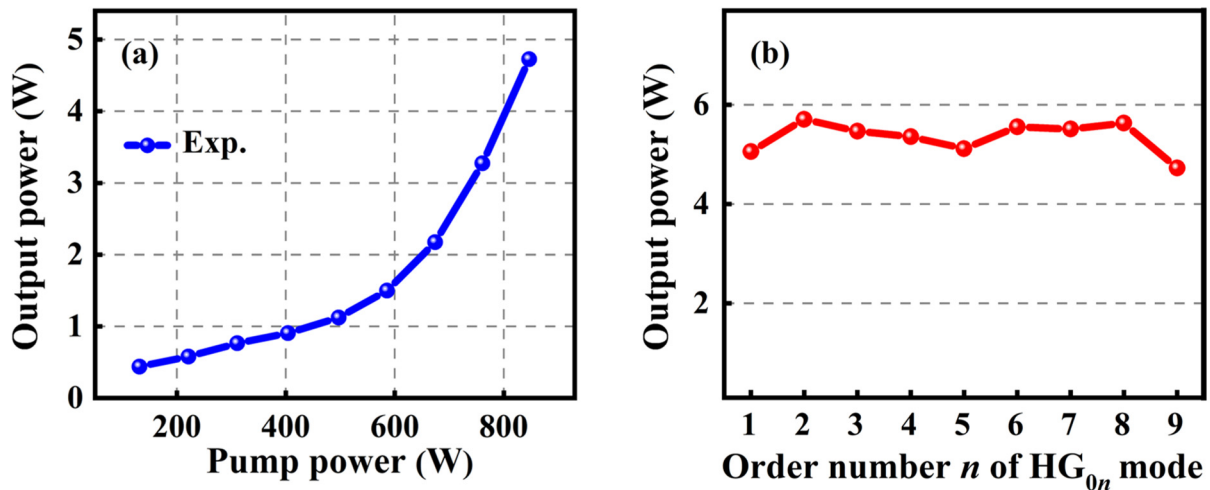
Figure 6. Measured amplified output power. (**a**) The output power for the highest HG_{09} mode versus pump power. (**b**) The amplified output power of the HG_{01} to HG_{09} modes.
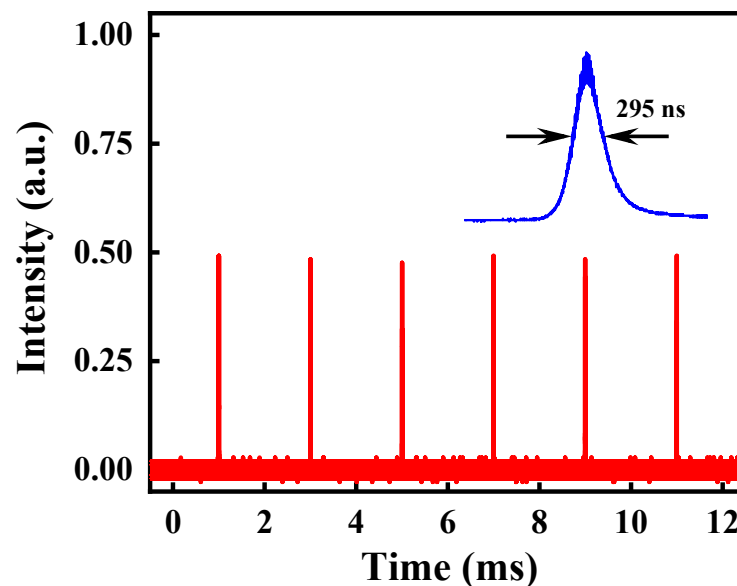

Figure 7. Oscilloscope traces of the pulse train (red line) for HG_{09} mode. Inset: expanded profile of a single pulse (blue line).

To expand the application, the following aspects, such as higher-order number n of the HG_{0n} mode, narrow pulse width, and the conversion to vortex LG_{pl} modes, will be the focus of our future work. In this paper, the 5 mm × 5 mm active aperture of the AO Q-switch limits the upper boundary of order number n, but with the use of the customized Q-switch with a larger aspect ratio aperture, HG_{0n} modes with order number n higher than 9 will be generated. Meanwhile, by replacing the AO Q-switch with a saturable absorber, the mode-locking can be obtained, and the pulse width can be reduced to several hundred picoseconds. Although previous studies have shown that ultrafast high-power HG_{mn} laser beams are affected by other parameters like self-phase modulation and bandwidth [25,26], the relatively large dimensions of the gain medium, such as a slab with a large aspect ratio, will reduce the effect. Further conversion to vortex LG_{pl} modes can be achieved by using AMC composed of cylindrical lenses, which will be widely used in optical communication, material processing, and many other fields [27–29].

5. Conclusions

In summary, we have proposed and demonstrated a new scheme for high-purity HG_{0n} laser beam generation and power scaling based on cascaded Nd:YAG slabs with a large aspect ratio. High-purity, ns HG_{0n} laser beams from HG_{01} to HG_{09} are first generated in a laser oscillator. The measured intensity distributions and beam quality factors align well with the theoretical predictions. After amplification, the average power of HG_{01} to HG_{09} modes is up to about 5 W, and for the highest order HG_{09} mode, the corresponding peak power is about 32 kW. To the best of our knowledge, these are both the highest average power and the highest peak power for high-purity, ns pulse HG_{0n} beams with continuously adjustable order. Hopefully, the scheme in this paper paves the way for high-power, high-purity, high-order HG_{0n} laser beam generation.

Author Contributions: Conceptualization, T.Y. and J.Y.; methodology, T.Y. and J.Y.; software, T.Y.; validation, T.Y., W.Z., Y.Z. and Z.Z.; formal analysis, T.Y. and J.Y.; investigation, W.Z. and X.L.; resources, Z.Z.; data curation, T.Y. and J.Y.; writing—original draft preparation, T.Y. and W.Z.; writing—review and editing, J.Y.; visualization, T.Y.; supervision, X.W.; project administration, J.Y., X.L. and X.W.; funding acquisition, J.Y., X.L. and X.W. All authors have read and agreed to the published version of the manuscript.

Institutional Review Board Statement: Not applicable.

Informed Consent Statement: Not applicable.

Data Availability Statement: The data presented in this paper can be obtained by contacting the corresponding author.

Conflicts of Interest: The authors declare no conflict of interest.

References

1. Sayan, O.F.; Gerçekcioğlu, H.; Baykal, Y. Hermite Gaussian beam scintillations in weak atmospheric turbulence for aerial vehicle laser communications. *Opt. Commun.* **2020**, *458*, 124735. [CrossRef]
2. Wang, P.X.; Ho, Y.K.; Tang, C.X.; Wang, W. Field structure and electron acceleration in a laser beam of a high-order Hermite-Gaussian mode. *J. Appl. Phys.* **2007**, *101*, 083113. [CrossRef]
3. Meena, H.K.; Singh, B.K. Experimental realization of modulated Hermite-Gaussian laser modes: A maximum number of highly intense lobes. *J. Opt. Soc. Am. A* **2021**, *39*, 2104–2109. [CrossRef] [PubMed]
4. Mitri, F.G. Cylindrical particle manipulation and negative spinning using a nonparaxial Hermite-Gaussian light-sheet beam. *J. Optics-UK* **2016**, *18*, 105402. [CrossRef]
5. Ghotra, H.S.; Jaroszynski, D.; Ersfeld, B.; Saini, N.S.; Yoffe, S.; Kant, N. Transverse electromagnetic Hermite-Gaussian mode-driven direct laser acceleration of electron under the influence of axial magnetic field. *Laser Part. Beams* **2018**, *36*, 154–161. [CrossRef]
6. Shen, Y.J.; Meng, Y.; Fu, X.; Gong, M.L. Wavelength-tunable Hermite–Gaussian modes and an orbital-angular-momentum-tunable vortex beam in a dual-off-axis pumped Yb:CALGO laser. *Opt. Lett.* **2018**, *43*, 291–294. [CrossRef]
7. Li, N.; Xu, B.; Cui, S.W.; Qiu, X.D.; Luo, Z.Q.; Xu, H.Y.; Cai, Z.P.; Chen, L.X.; Moncorgé, R. High-order vortex generation from CW and passively Q-switched Pr:YLF visible lasers. *IEEE Photonics Technol. Lett.* **2019**, *31*, 1457–1460. [CrossRef]
8. Huang, X.X.; Xu, B.; Cui, S.W.; Xu, H.Y.; Cai, Z.P.; Chen, L.X. Direct generation of vortex laser by rotating induced off-axis pumping. *IEEE J. Sel. Top. Quant.* **2018**, *24*, 1–6. [CrossRef]
9. Zhang, J.; Yu, X.Y.; Chen, Y.Q.; Huang, M.; Dai, X.; Liu, D. Generation of Hermite-Laguerre-Gaussian beams based on space-variant Pancharatnam Berry phase. *Proc. SPIE* **2018**, *10964*, 109645R.
10. Ma, L.; Guo, H.; Sun, H.; Liu, K.; Su, B.; Gao, J. Generation of squeezed states of light in arbitrary complex amplitude transverse distribution. *Photonics Res.* **2020**, *8*, 1422–1427. [CrossRef]
11. Dong, J.; He, Y.; Bai, S.C.; Ueda, K.; Kaminskii, A. A Cr^{4+}:YAG passively Q-switched Nd:YVO4 microchip laser for controllable high-order Hermite–Gaussian modes. *Laser Phys.* **2016**, *26*, 095004. [CrossRef]
12. Zhang, M.M.; He, H.S.; Dong, J. Decentered Gaussian beam pumped highly efficient passively Q-switched microchip laser for controllable high-order transverse modes. *IEEE Photonics J.* **2017**, *9*, 1501214. [CrossRef]

13. Hnatovsky, C.; Shvedov, V.G.; Krolikowski, W.; Rode, A.V. Materials processing with a tightly focused femtosecond laser vortex pulse. *Opt. Lett.* **2010**, *35*, 3417–3419. [CrossRef]
14. Luo, Z.; Wang, C.; Dong, X.R.; Duan, J.A. Femtosecond laser highly-efficient plane processing based on an axicon-generated donut-shaped beam. *Chin. Opt. Lett.* **2018**, *16*, 031401.
15. Demirci, E.; Nolke, C.; Kaierle, S.; Matteazzi, P. Development of a hollow laser beam for micromachining. *Adv. Opt. Technol.* **2012**, *1*, 365–370. [CrossRef]
16. Zhang, L.; Guo, Y.D.; Chen, Z.Z.; Gong, K.L.; Xu, J.L.; Yuan, L.; Lin, Y.D.; Meng, S.; Li, Y.; Shao, C.F.; et al. A near 60% efficiency single-slab Nd:YAG high-power laser with adjustable pulse duration. *IEEE Photonics Tech. Lett.* **2019**, *31*, 405–408. [CrossRef]
17. Liu, Y.; Lei, J.; Li, T.Q.; Li, N.; Tang, X.J. 4.55 kW LD end-pumped Nd:YAG surface gain slab laser. *Laser Phys.* **2019**, *29*, 016101. [CrossRef]
18. Guo, Y.D.; Peng, Q.J.; Bo, Y.; Chen, Z.Z.; Li, Y.; Zhang, L.; Shao, C.F.; Yuan, L.; Wang, B.S.; Xu, J.; et al. 24.6 kW near diffraction limit quasi-continuous-wave Nd:YAG slab laser based on a stable–unstable hybrid cavity. *Opt. Lett.* **2020**, *45*, 1136–1139. [CrossRef]
19. Beijersbergen, M.W.; Allen, L.; van der Veen, H.E.L.O.; Woerdman, J.P. Astigmatic laser mode converters and transfer of orbital angular momentum. *Opt. Commun.* **1993**, *96*, 123–132. [CrossRef]
20. Koechner, W. *Solid-State Laser Engineering*, 6th ed.; Springer: New York, NY, USA, 2006; pp. 163, 224–228.
21. McCumber, D.E. Eigenmodes of a symmetric cylindrical confocal laser resonator and their perturbation by output-coupling apertures. *Bell Syst. Tech. J.* **1965**, *44*, 333–363. [CrossRef]
22. Freiberg, R.J.; Halsted, A.S. Properties of low order transverse modes in argon ion lasers. *Appl. Opt.* **1969**, *8*, 355–362. [CrossRef] [PubMed]
23. Di, P.C.; Li, X.P.; Yang, J.; Wang, R.J.; Wang, X.J.; Liu, K.; Cui, D.F.; Peng, Q.J. High-power VCSEL-pumped slab laser with temperature fluctuation adaptability. *IEEE Photonics Tech. Lett.* **2021**, *33*, 395–398. [CrossRef]
24. Siegman, A.E.; Townsend, S.W. Output beam propagation and beam quality from a multimode stable-cavity laser. *IEEE J. Quantum Electron.* **1993**, *29*, 1212–1217. [CrossRef]
25. Tawfik, W. High-power table-top white-light few-cycle laser generator. *Ukr. J. Phys. Opt.* **2015**, *16*, 111–119. [CrossRef] [PubMed]
26. Tawfik, W. Reaching white-light radiation source of ultrafast laser pulses with tunable peak power using nonlinear self-phase modulation in neon gas. *Radiat. Phys. Chem.* **2016**, *125*, 165–170. [CrossRef]
27. Wang, J. Advances in communications using optical vortices. *Photon. Res.* **2016**, *4*, 14–28. [CrossRef]
28. Woerdemann, M.; Alpmann, C.; Esseling, M.; Denz, C. Advanced optical trapping by complex beam shaping. *Laser Photonics Rev.* **2013**, *7*, 839–854. [CrossRef]
29. Padgett, M.; Bowman, R. Tweezers with a twist. *Nat. Photonics* **2011**, *5*, 343–348. [CrossRef]